Revista Mexicana de Astronomía y Astrofísica, **44**, 161–170 (2008)

HII REGIONS IN NGC 5055. II. PHYSICAL PROPERTIES

M. Rozas

Instituto de Astronomía
Universidad Nacional Autónoma de México, Ensenada, B. C., Mexico

Received 2007 September 13; accepted 2008 January 21

RESUMEN

En este artículo usamos las observaciones presentadas en Rozas (2007) de la galaxia NGC 5055 en las líneas Hα y Hβ, junto con observaciones CCD con filtros estrechos en las líneas [OII], [OIII], [SII] y S[III] para calcular las anchuras equivalentes, excitación, grados de ionización, parámetros de ionización y metalicidades de las regiones catalogadas en Rozas (2007).

ABSTRACT

In this paper, using CCD observations of the galaxy NGC 5055 in the emission lines of Hα and Hβ (Rozas 2007), together with CCD observations in the narrow-band filters of [OII], [OIII], [SII], and S[III] lines we have calculated the equivalent widths, excitations, ionization hardness, ionization parameters and metallicities for the regions catalogued in Rozas (2007).

Key Words: galaxies: individual (NGC 505) — galaxies: kinematics and dynamics — galaxies: spiral

1. INTRODUCTION

We obtained images of the spiral galaxy NGC 5055 during the nights of 2005 June 14th–18th, with the 0.84 m telescope of the Observatorio Astronómico Nacional in the Sierra San Pedro Mártir. We obtained the images using narrow band filters for the wavelengths Hα, Hβ, [OII]$\lambda\lambda$ 3726, 3729, [OIII] λ5007, [SII]$\lambda\lambda$ 6717, 6731 and [SIII]λ 9069 and their respective continuum filters. In Rozas (2007, hereafter Paper I) we catalogued 372 HII regions and calculated their statistical properties: the luminosity function and the geometrical distributions. In this second paper we present the physical properties of the HII regions catalogued: their equivalent widths, excitationss, ionization hardness, ionization parameters and metallicities.

In Figure 1 of Paper I we show a grey scale representation of the Hα image of NGC 5055. The spiral arms show up as a grainy background, which brightens slowly from the periphery to the nuclear region, which is still grainy. Star forming regions can be traced along the spiral arms. NGC 5055 has been studied previously in ^{12}CO (J=1-0) by Tosaki et al. (2002) and in HI by Battaglia et al. (2006). These authors note the regularity and symmetry of the galaxy, but a mild lopsidedness is noticeable, both in the distribution and the kinematics of the gas. The tilted ring analysis of the velocity field suggests a range of values for the kinematical center and different systemic velocities for the inner and the outer parts of the system. This implies a remarkable result: the kinematical and geometrical asymmetries disappear, both at the same time. These results point to two different dynamical regimes: an inner region dominated by the stellar disk and an outer region dominated by a dark matter halo, offset with respect to the disk.

In this paper we aim to complete these earlier studies by observing a significant number of HII regions in several emission lines in order to be able to extract conclusions about the star formation trends that occur in spiral galaxies.

2. OBSERVATIONS AND DATA REDUCTION

The observations and data reduction procedures for the Hα and Hβ images are summarized in § 2 of Paper I. The observations of NGC 5055 in the other lines were made during the same nights of June 14th–18th 2005 with the 0.84 m telescope of the Observatorio Astronómico Nacional in the Sierra San Pedro Mártir. The detector was a Site 1 CCD. The projected pixel size was 0.39″/pix. The observing

TABLE 1

FILTERS USED AND EXPOSURE TIMES

OII	3725	5 × 1500 s
OII cont	3500	1800 s
OIII	5012	5 × 1500 s
OIII cont	5470	1800 s
SII	6737	6 × 1800 s
SII cont	7157	3 × 1500 s
SIII	9150	8 × 1500 s
SIII cont	8510	4 × 1500 s

conditions were very good with 1″ seeing and a photometric sky.

Table 1 shows the filters used and the exposure times. The first column lists the name of the filter, the second column contains the central wavelength for each filter in angstroms, and the last columns indicates the exposure time employed for each filter. Standard reduction routines were used, closely following the procedure of previous studies. A bias level was first subtracted, and the images were then corrected using appropriate dawn sky flatfields. Next, a value for the sky background was obtained by measuring the background and the associated noise levels in portions of the image where there was no emission from the galaxy. In order to align the two images (line and continuum images), positions of several foreground stars were determined based upon Gaussian fits, and the off-band images were displaced to coincide with the on-band images. The accuracy of the superpositions was better than 0.3 pixels in all cases.

Once the aligned images were cleaned of cosmic rays and of the occasional bad pixels, the continuum images were subtracted from the line image, giving net fluxes. To subtract the continuum, all the continuum images were multiplied by factors that turned out to be close to unity. These factors were determined assuming that the inter-arm emission was null after the subtraction. This was preferred to the field star method, because these stars may present different spectral energy distributions from that of the stellar population of the galaxy, and also they may present strong absorption lines, so the correction factors will be underestimated or overestimated. Moreover, using this method we are able to correct every line for diffuse background emission. Figures 1–4 present the resulting emission line images for NGC 5055 in [OII], [OIII], [SII] and [SIII].

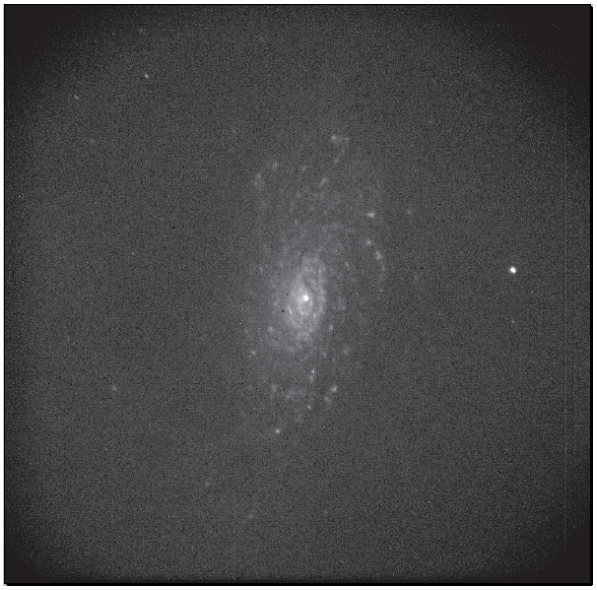

Fig. 1. Grey scale representation of the [OII] continuum-subtracted image of NGC 5055.

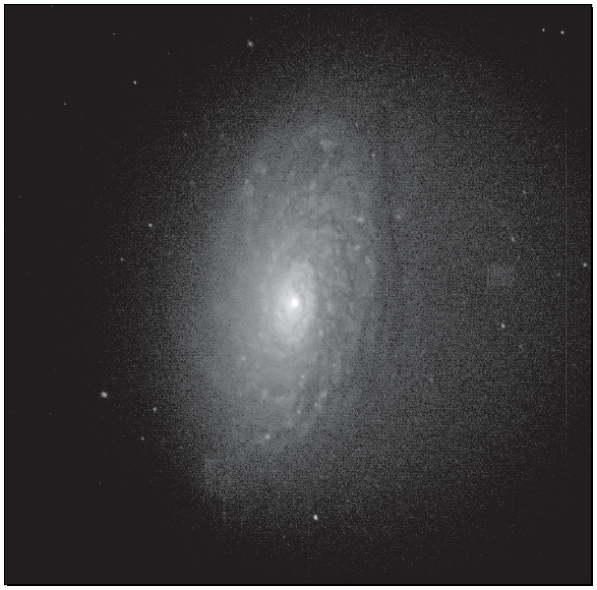

Fig. 2. NGC 5055 [OIII] continuum subtracted.

In Paper I, we explained the procedure to carry out a correction for the effect of galactic and extragalactic extinction using the ratio of the Hα and Hβ fluxes.

3. RESULTS

Table 2 summarizes the flux for several emission lines for NGC 5055. Columns 1, 6 and 11 list the

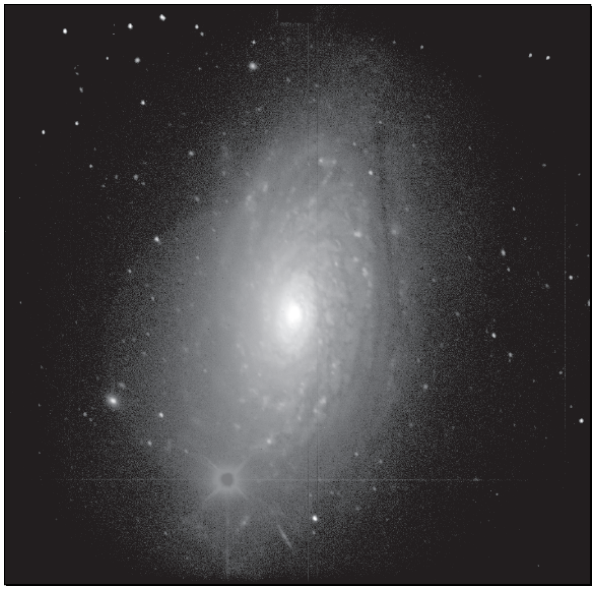

Fig. 3. NGC 5055 [SII] continuum subtracted.

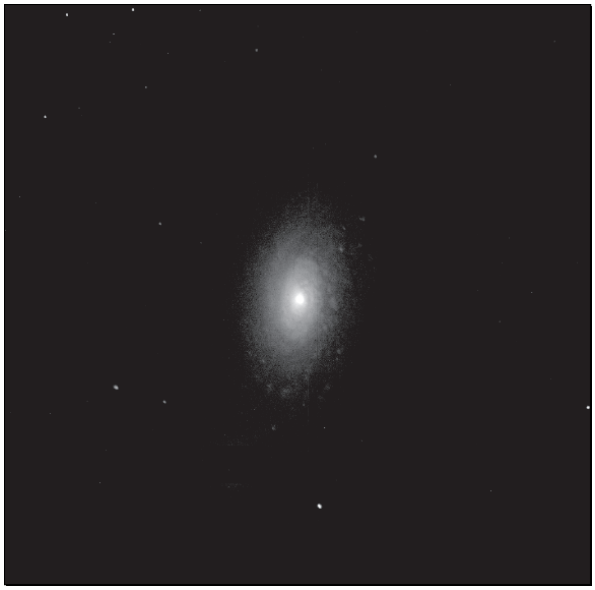

Fig. 4. NGC 5055 [SIII] continuum subtracted.

identification number of the region. Columns 2–5, 7–10 and 12–15 list the[OII], [OIII], [SII] and [SIII] ratios with respect to Hβ. All the quantities are relative to Hβ=100 and are corrected for extinction. We have assumed the theoretical relations: I([OIII]$\lambda\lambda$4959,5007)=1.34 I([OIII]λ 5007) and I([SIII]$\lambda\lambda$ 9069,9532)=3.43 I([SIII]λ 9069).

In Table 3 we summarize several quantities derived for the line ratios. Columns 1, 4 and 9 list the region identification number, Columns 2, 5 and 10 the R_{23} parameter defined by Pagel et al. (1979):

$$R_{23} = \frac{I([OII]\lambda 3727) + I([OIII]\lambda\lambda 4959, 5007)}{I(H\beta)} \quad (1)$$

This parameter is an empirical oxygen abundance indicator when the temperature-sensitive lines, such as [OIII]λ4363, are unavailable. Columns 3, 6 and 11 list the oxygen abundance derived from the calibration of Zaritsky, Kennicutt, & Huchra (1994):

$$\begin{aligned} 12 + \log(O/H) &= 9.265 - 0.33x - 0.202x^2 \\ &\quad -0.207x^3 - 0.333x^4\,, \end{aligned} \quad (2)$$

where $x = \log R_{23}$.

Columns 4, 7 and 12 list the η parameter defined as:

$$\eta = \frac{[OII]\lambda\lambda 3726, 3729/[OIII]\lambda\lambda 4959, 5007}{[SII]\lambda\lambda 6717, 6731/[SIII]\lambda\lambda 9069, 9532} \quad (3)$$

This parameter scales roughly with the actual ionic ratios of oxygen and sulfur and, hence, provides an indicator of the hardness of the ionizing spectrum. This parameter does not depend strongly upon the electron temperature or density, or upon the reddening. It is related to the γ parameter (Vílchez & Pagel 1988),

$$\gamma = \frac{O^+/O^{++}}{S^+/S^{++}} \quad (4)$$

via the relation:

$$\log\gamma = \log\eta + \frac{0.14}{t} + 0.16\,, \quad (5)$$

where $t = T_e/10^4$, T_e being the electron temperature. Furthermore, it assumes the low density limit for ionic emissivities and ignores any temperature fluctuactions.

3.1. *Extinction*

To obtain the values for the extinction, we employed the relation given in Paper I, equation (1):

$$A_V = 2.5 \ln \frac{(F H\alpha / F H\beta)_{\rm observed}}{2.86} \quad (6)$$

Figure 5 shows a histogram representing the number of regions with different extinction values. The mean value obtained for the extinction is A_V=0.81 mag. There are many regions with values for the extinction close to 1.0 mag and distributed in a somewhat Gaussian form.

TABLE 2

NGC 5055 [OII],[OIII], [SII] AND [SIII] FLUXES

Region	OII	OIII	SII	SIII	Region	OII	OIII	SII	SIII	Region	OII	OIII	SII	SIII
1	213	48	73		64	188	114	64		127	206	36	45	
2	267	39	44		65		16	38		128	326	121	75	
3	203	110	25		66	236	46	76		129	223	94	36	
4	155	54	36		67	261	107	64		130	359	67	43	
5	204	54	83	128	68			14	24	131	117	35	39	
6		13	54		69	64	29	31		132		37	39	
7		11	16		70	90	26	53		133			25	
8	184	44	57		71	441	128	74		134	306	39	46	
9	153	33	35		72	116	38	45		135		19	36	
10	307	158	57	44	73	105	26	44		136		24	43	
11		33	54		74	252	191	98		137	329	89	108	
12	189	54	64		75	154	58	43		138	231	73	44	
13	141	32	67		76	86	19	38		139	197	54	55	
14	126	35	73		77	207	103	54		140	335	115	77	
15	85	49	55		78	112	79	109		141	242	22	79	
16	279	96	88		79	292	261	66	29	142	196	49	77	
17	84	22	44		80	383	71	49		143	165	37	67	
18			35		81	133	37	75		144	267	43	77	
19			56		82	290	194	38		145	325	58	65	
20	105	66	53		83	294	57	76		146	136	28	48	
21	352	139	59		84	284	216	23		147		19	24	
22	335	43	77		85	214	57	49		148	196	42	77	
23	155	44	57		86	274	107	52		149	177	41	69	
24	130	23	80		87	490	43	177		150	198		79	
25		37	48		88	115	79	111		151	63	19	57	
26	146	23	46		89	266	63	103		152	157	26	39	
27		78	47		90	350	271	37		153	213	78	39	
28	591	95	70		91	302	106	56		154	228	96	48	
29	178	45	77	80	92	175	44	79		155		24	39	
30	184	59	57		93	112	29	33		156		19	52	
31	179	49	69		94	389	147	96		157	156	27	59	
32		35	38		95	373	45	89		158	196	36	43	
33	287	30	71		96	380	73	54		159	75	29	44	
34		43	38		97	373	126	51		160	215	28	69	
35	253	72	55		98	158	22	48		161	148	55	75	
36		27	55		99			38		162	318	43	66	
37		8	33		100	617	126	144		163	290	36	71	
38	169	86	44		101	235	171	44		164	256	49	71	
39	235	68	54	88	102			90		165			38	
40	293	136	31		103	266	147	23		166	163	44	57	
41		14	23		104	246	169	129		167		69	25	
42	219	26	58		105	144	18	54		168	223	55	64	
43	271	35	55		106	184	43	48		169	264	86	66	
44	243	142	80		107	305	111	53	325	170	262	124	43	
45			66		108	395	91	45		171	374	93	124	
46	375	118	86		109		34	48		172	180	46	76	
47	108	35	49		110					173	189	83	67	
48			42		111	349	73	49		174	95	37	66	
49	481	102	37		112	234	87	84		175	155	60	77	
50	194	42	36		113	216	46	55		176	760		127	
51		34			114	235	39	61		177	416	226	56	
52	321	43	35		115	217	247	38		178	238	76	39	
53	105	42	65		116	141	37	68		179	317	220	58	
54	209	35	75		117	121	25	65		180	162	43	74	
55		21	26		118	123	16	56		181		19	49	
56	186	106	66		119		14	39		182	380	96	53	
57	282	45	48		120	328	78			183	118	26	55	
58	185	74	36		121			48		184			39	
59	93	27	14		122	125	20	61		185			48	
60	212	175	137		123	383	53	57		186	236	46	48	
61	126	38	56	119	124	245	25	46		187	319	56	66	
62		125	66		125	187	24	76		188	444	27	39	
63	173	32	68		126	264	135	65		189	219	66	67	

TABLE 2 (CONTINUED)

Region	OII	OIII	SII	SIII	Region	OII	OIII	SII	SIII	Region	OII	OIII	SII	SIII
190	188	9	62		219	205	82	18		247		13	19	
191	298	67	44		220	224	85	48	76	248	320	69	60	
192		25	54		221	64	24	17		249		15	21	
193	195	53	77		222	233	81	105		250	89	22	37	
194			34		223	264	32	105		251	221	36	36	
195	302	83	75		224	16	9	23		252	152	13	43	
196	93	27	34		225	284	39	58		253	246	62	70	119
197			36		226	165	29	31		254		23	28	
198	192	54	49		227	203	45	52		255			25	
199			69		228	168	32	47		256	64	89		
200	69	25	56		229			308		257		68	51	
201	306	56	72		230	309	61	53		258		18	31	
202	127	46	70		231		24	23		259		17	35	
203			45		232	75	39	22		260	146	55	31	
204	286	126	35		233	185	49	75		261	298	71	99	
205			32		234	156	33	46		262	139		68	
206	166	69	13	65	235		69	43		263	146	37	69	
207	163	36	57	130	236	139	26	16		264	333	47	77	
208		41	23		237	27	7	14		265	306	153	54	
209	274	56	58		238	213	66	44		266	185	100	61	
210	48	23	47		239	63	89			267	258	77	50	
211	201	30	25		240		7	30		268	204	37	77	
212		25	86		241		30	40		269	168	83	48	
213	273		83		242			21		270	210	175	136	
214	136	27	35		243	138	28	42		271	110	75	106	
215	68	19	12		244		21	25		272	86	19	39	
216	191	72	22		245			14		273	216	27	67	
217	310	43	48		246	143	30	48		274	205	45	51	
218			23											

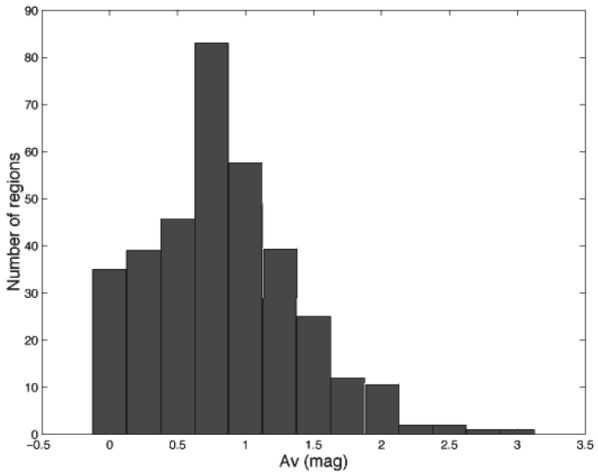

Fig. 5. Histogram for extinction in NGC 5055.

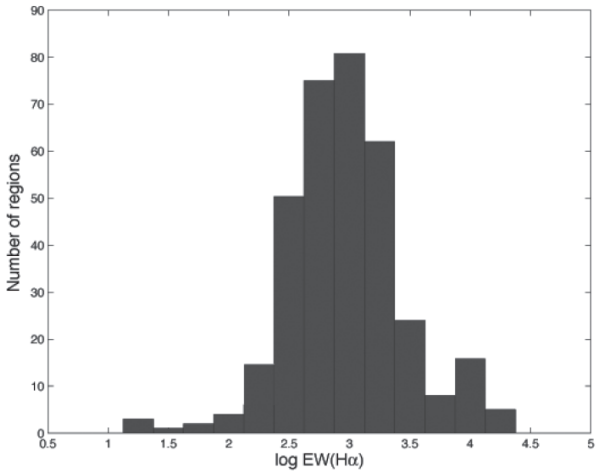

Fig. 6. Histogram for log of Hα equivalent width in NGC 5055.

3.2. *Equivalent widths*

The Hα equivalent width provides a measure of the ratio of ionizing photons from massive stars and continuum photons from the embedded stars and gas. For this reason, this parameter is sensitive to variations of the initial mass function (IMF), the evolutionary stage of ionizing stars and their metallicity (Leitherer et al. 1999; Kennicutt, Keel, & Blha 1989; Martin & Friedli 1999; Bresolin & Kennicutt 1997). Generally, the EW(Hα) in disc galaxies goes from 100 Å to 1500 Å, with a mean value of 400 Å.

In Figure 6 we show the histogram for the logarithm of the Hα equivalent width for HII regions in NGC 5055. The mean value for this galaxy is

TABLE 3

NGC 5055 R_{23} PARAMETER, OXYGEN ABUNDANCE AND IONIZATION HARDNESS PARAMETER

Region	R_{23}	12+log(O/H)	η	Region	R_{23}	12+log(O/H)	η	Region	R_{23}	12+log(O/H)	η
1	2.63	9.09		64	2.98	9.05		127	2.38	9.08	
2	3.13	9.02		65				128	4.62	8.84	
3	3.10	9.01		66	2.88	9.06		129	3.23	9.01	
4	2.04	9.13		67	3.71	8.95		130	4.21	8.88	
5	2.50	9.05	0.77	68				131	1.41	9.22	
6				69	0.97	9.26		132			
7				70	1.24	9.23		133			
8	2.23	9.13		71	5.66	8.67		134	3.43	8.98	
9	1.85	9.19		72	1.56	9.19		135			
10	4.60	8.80	0.19	73	1.37	9.21		136			
11				74	4.48	8.84		137	4.17	8.89	
12	2.40	9.09		75	2.07	9.13		138	3.10	9.00	
13	1.77	9.17		76	1.06	9.26		139	2.43	9.08	
14	1.65	9.19		77	3.09	9.02		140	4.52	8.85	
15	1.37	9.25		78	1.91	9.16		141	2.63	9.09	
16	3.72	8.94		79	5.63	8.72	0.33	142	2.43	9.10	
17	0.96	9.27		80	4.63	8.82		143	2.05	9.13	
18				81	1.66	9.16		144	3.00	9.02	
19				82	4.94	8.79		145	3.82	8.94	
20	1.65	9.19		83	3.46	8.95		146	1.64	9.19	
21	4.85	8.85		84	4.95	8.81		147			
22	3.73	8.94		85	2.65	9.06		148	2.43	9.08	
23	1.94	9.17		86	3.77	8.95		149	2.15	9.13	
24	1.58	9.16		87	5.37	8.76		150			
25				88	1.92	9.15		151	0.84	9.28	
26	1.65	9.17		89	3.19	9.02		152	1.77	9.17	
27				90	6.25	8.66		153	2.84	9.03	
28	6.96	8.57		91	3.99	8.91		154	3.22	9.00	
29	2.17	9.13	0.65	92	2.13	9.13		155			
30	2.38	9.11		93	1.45	9.22		156			
31	2.26	9.13		94	5.27	8.77		157	1.76	9.18	
32				95	4.11	8.89		158	2.36	9.08	
33	3.26	8.99		96	4.63	8.82		159	0.95	9.26	
34				97	5.07	8.77		160	2.34	9.10	
35	3.36	8.97		98	1.76	9.18		161	1.95	9.15	
36				99				162	3.57	8.97	
37				100	7.32	8.50		163	3.26	8.99	
38	2.44	9.06		101	4.13	8.87		164	3.05	9.03	
39	2.95	9.01	0.72	102				165			
40	4.27	8.87		103	4.14	8.88		166	2.13	9.12	
41				104	4.08	8.89		167			
42	2.31	9.12		105	1.55	9.18		168	2.75	9.06	
43	3.03	9.02		106	2.25	9.11		169	3.56	8.98	
44	3.90	8.90		107	4.15	8.89	1.26	170	3.96	8.92	
45				108	4.92	8.81		171	4.68	8.85	
46	5.03	8.76		109				172	2.24	9.12	
47	1.45	9.22		110				173	2.64	9.06	
48				111	4.19	8.89		174	1.34	9.21	
49	5.95	8.69		112	3.20	9.00		175	2.19	9.13	
50	2.33	9.11		113	2.51	9.06		176			
51				114	2.65	9.05		177	6.52	8.61	
52	3.66	8.97		115	4.66	8.85		178	3.09	9.02	
53	1.51	9.22		116	1.79	9.18		179	5.55	8.74	
54	2.42	9.08		117	1.49	9.23		180	2.01	9.11	
55				118	1.33	9.22		181			
56	2.88	9.02		119				182	4.80	8.80	
57	3.33	8.98		120	4.02	8.91		183	1.44	9.22	
58	2.55	9.06		121				184			
59	1.24	9.25		122	1.43	9.23		185			
60	3.85	8.92		123	4.46	8.86		186	2.76	9.05	
61	1.68	9.19	0.86	124	2.67	9.09		187	3.74	8.92	
62				125	2.07	9.14		188	4.74	8.83	
63	2.03	9.15		126	3.99	8.92		189	2.85	9.05	

TABLE 3 (CONTINUED)

Region	R_{23}	12+log(O/H)	η	Region	R_{23}	12+log(O/H)	η	Region	R_{23}	12+log(O/H)	η
190	2.36	9.12		219	2.83	9.06		247	1.62	9.16	
191	3.67	8.97		220	3.12	9.03	0.62	248	2.03	9.15	
192				221	0.81	9.28		249	1.67	9.19	
193	2.46	9.06		222	3.22	9.02		250	1.13	9.25	
194				223	2.90	9.03		251	3.85	8.93	
195	3.84	8.90		224	0.22	9.39		252	2.11	9.13	
196	1.20	9.24		225	3.27	8.98		253	1.18	9.26	
197				226	1.88	9.15		254	0.90	9.27	
198	2.42	9.09		227	2.51	9.09		255	1.88	9.14	
199				228	1.92	9.12		256			
200	0.98	9.28		229				257	1.57	9.18	
201	3.64	8.94		230	3.66	8.93		258	1.96	9.16	
202	1.65	9.18		231				259	2.55	9.09	
203				232	1.14	9.23		260	1.98	9.15	
204	4.07	8.87		233	2.28	9.13		261	2.81	9.03	
205				234	1.84	9.15		262	1.54	9.19	
206	2.23	9.12	0.64	235				263	2.59	9.07	
207	2.09	9.14	1.03	236	1.65	9.19		264	3.34	8.99	
208				237	0.31	9.38		265	2.35	9.11	
209	3.39	8.99		238	2.85	9.04		266	4.93	8.82	
210	0.63	9.31		239				267	2.35	9.11	
211	2.38	9.11		240				268	5.92	8.68	
212				241				269	3.75	8.93	
213				242	1.37	9.21		270	5.73	8.72	
214	1.67	9.19		243	1.56	9.19		271	4.14	8.89	
215	0.81	9.28		244	1.66	9.16		272	3.78	8.95	
216	2.68	9.05		245	1.67	9.19		273	2.41	9.09	
217	3.59	8.98		246	1.04	9.26		274	2.51	9.08	
218											

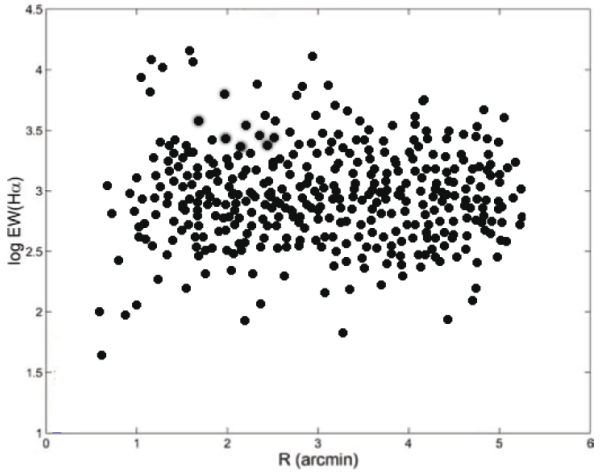

Fig. 7. Hα equivalent width as a function of galactocentric radius for NGC 5055.

log(EW[Hα])=3.15, which is equivalent to an age of between 1.6 and 4 Myr, depending upon the IMF selected (using Leitherer et al. 1999 models).

Figure 7 shows the Hα equivalent width for the HII regions as a function of galactocentric radius for NGC 5055. The general trend is an almost constant value for the equivalent width with the radius, which indicates that the diffuse emission from the disc was successfully removed.

3.3. *Excitation*

The HII regions can be classified as "high excitation" or "low excitation" in terms of large or small values of the ratio [OIII]/Hβ=I($\lambda\lambda$5007,4959)/I(λ4861) (Aller 1942; Searle 1971). Empirically, strong [OIII] lines are related to low oxygen abundances, high gas temperatures and a large values of $X(O^{+2})$, where X is a nebular average (Searle 1971; Smith 1975; Shields 1990). Figure 8 shows the excitation as a function of galactocentric radius for NGC 5055. The figure indicates that the excitation increases with radius. This increase in the excitation can be explained as an effect of the metallicity gradient that will be discussed later.

Figure 9 shows the correlation between log([OII]/Hβ) and the log of the excitation for each HII region of the galaxy. As we can see, the HII regions of NGC 5055 cover all the excitation range, with regions of low excitation in the inner parts of the galaxy and high excitation in the outer parts.

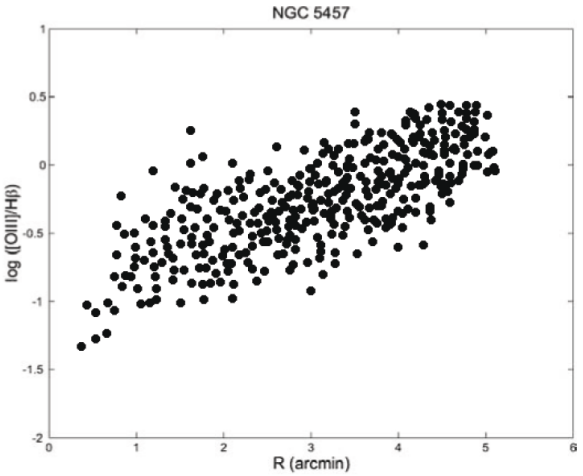

Fig. 8. Excitation as a function of galactocentric radius for NGC 5055.

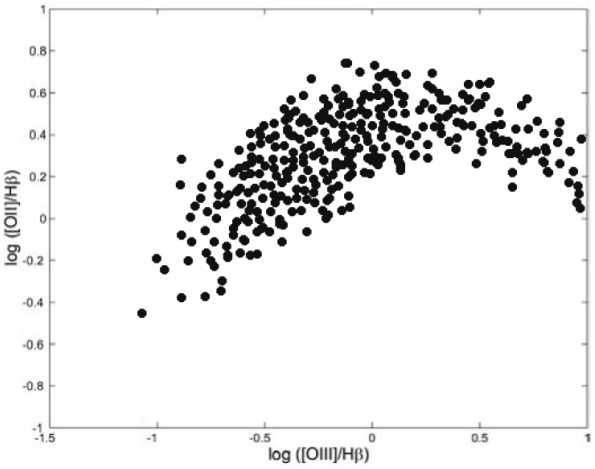

Fig. 9. Correlation between log([OII]/Hβ) and the logarithm of excitation.

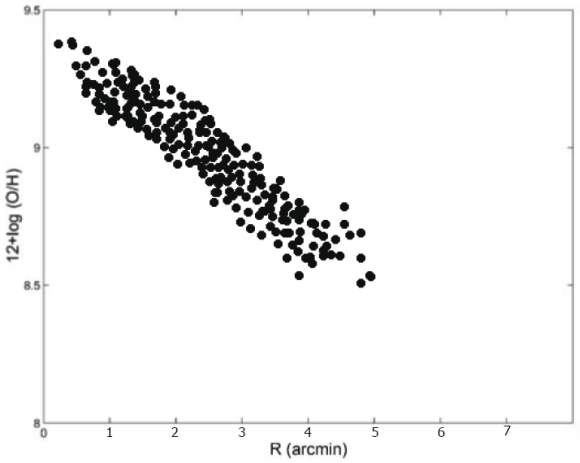

Fig. 10. Metallicity for NGC 5055.

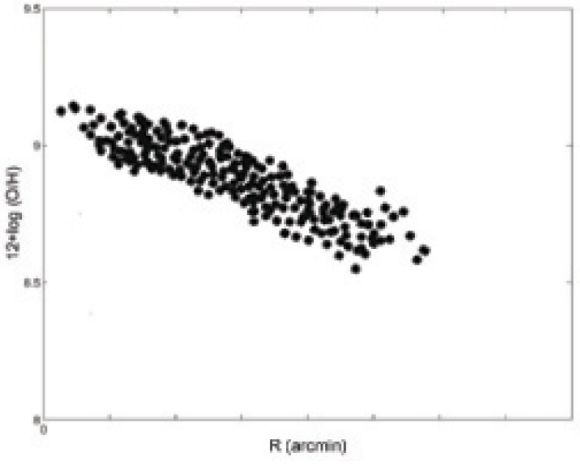

Fig. 11. Correlation between log([OII]/Hβ) and the logarithm of excitation.

According to McCall, Rybski, & Shields (1985), the clear correlation between log([OII]/Hβ) and log([OIII]/Hβ) and the low dispersion of the data implies that the majority of the HII regions are ionization bounded.

3.4. *Metallicity*

As was indicated above, we obtained the metallicity using the calibration given by Zaritsky et al. (1994), based upon the R_{23} parameter. This estimator is precise to about 0.2 dex (Pagel, Edmunds, & Smith 1980), and it is double-valued in the range $0.9 < \log R_{23} < 1$, which introduces more uncertainties in the metallicity determination for HII regions with these values of log R_{23}. However, only a few of the HII regions present values exceeding 0.85.

In Figure 10 we show the values of the metallicity versus the deprojected radius for NGC 5055. We can see that there is a very steep gradient in its inner parts, from 12+log(O/H)=9.4 to 12 log(O/H)=8.5. As van Zee et al. (1998) and Cedrés & Cepa (2002) have pointed out, this happens because the analytical form of the calibration does not explicitly take into account the turnover in R_{23}, so it can result in artificially high abundances for the inner HII regions.

For comparison, in Figure 11, we show the values of the metallicity versus the deprojected radius using a more modern calibration (Pilyugin 2007). Here, we can see that the results obtained using the calibration from Zaritsky et al. (1994) are larger that the metallicities obtained using this calibration and the gradient is smaller.

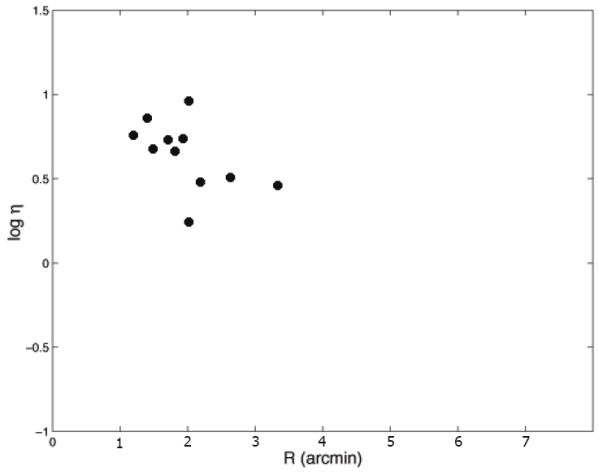

Fig. 12. Ionization hardness as a function of galactocentric radius for NGC 5055.

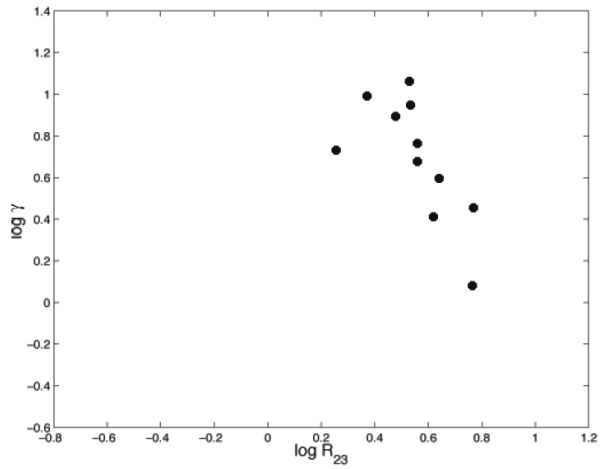

Fig. 13. Relation between log η and log R_{23} for NGC 5055.

3.5. *Ionization hardness*

According to Christensen, Petersen, & Gammelgaard (1997), Bresolin, Kennicutt, & Garnett (1999), and Garnett (1989), the ionization hardness parameter, η, can be used to study trends in the temperature of the ionizing clusters, because there is a direct relation between η and the temperature.

To derive this parameter, we have to observe at least the [SIII]λ9069 line. However, this emission line is rather weak and it falls on a region where the sensitivity of the CCD starts to drop. For this reason, observations of the [SIII] lines are available for only a few regions in NGC 5055.

In Figure 12 we plot the η parameter as a function of galactocentric radius for NGC 5055. Although our data in [SIII] have very large uncertainties, there is a clear relation between the two quantities, with η decreasing as a function of radius. Such gradients have been previously found by Vílchez & Pagel (1988); Zaritsky et al. (1994), and Cedrés & Cepa (2002) for other galaxies. This can be interpreted as a trend in the effective temperature of ionizing stars: the temperature is lower in the inner part of the galaxy and higher in the outer part, as was previously pointed out by Christensen et al. (1997), Bresolin et al. (1999) or Garnett (1989).

In Figure 13 we plot the logarithm of the ionization hardness parameter as a function of the logarithm of the abundance parameter R_{23}. Here, we also have a clear relation between both quatities, with a hardenning of the radiation as log R_{23} decays, which implies an increase in metallicity.

4. CONCLUSIONS

Using the catalogue of the HII regions of NGC 5055 compiled in Paper I, in conjunction with narrow-band images in the lines of Hα, Hβ, [OII], [OIII], [SII], and [SIII], we calculated several physical properties of the HII regions in this galaxy, which we can summarize as follows:

- We have measured the extinction for the HII region in the galaxy using the Hα/Hβ ratio. The mean value for the extinction is of $A_V = 0.81$ mag.
- We also mesured the Hα equivalent widths for each HII region.
- We have measured the excitation for each HII region in NGC 5055. This quantity presents a clear gradient.
- Using a semiempirical calibration proposed by Zaritsky et al. (1994), we have derived the metallicity using strong oxygen lines. We find a clear gradient in the inner parts of the galaxy. We also show the values of the metallicity versus the deprojected radius using another calibration (Pilyugin 2007). With this calibration we can see that the results obtained using the calibration from Zaritsky et al. (1994) are larger, and that the gradient is smaller.

REFERENCES

Aller, L. H. 1942, ApJ, 95, 52
Battaglia, G., Fraternali, F., Oosterloo, T., & Sancisi, R. 2006, A&A, 447, 49
Bresolin, F., & Kennicutt, R. C., Jr. 1997, AJ, 113, 975
Bresolin, F., Kennicutt, R. C., Jr., & Garnett, D. R. 1999, ApJ, 510, 104

Cedrés, B., & Cepa, J. 2002, A&A, 391, 809
Christensen, T., Petersen, L., & Gammelgaard, P. 1997, A&A, 322, 41
Garnett, D. R. 1989, ApJ, 345, 282
Kennicutt, R. C., Jr., Keel, W. C., & Blaha, C. A. 1989, AJ, 97, 1022
Leitherer, C., et al. 1999, ApJS, 123, 3
Martin, P., & Friedli, D. 1999, A&A, 346, 769
McCall, M. L., Rybski, P. M., & Shields, G. A. 1985, ApJS, 57, 1
Pagel, B. E. J., Edmunds, M. G., Blackwell, D. E., Chun, M. S., & Smith, G. 1979, MNRAS, 189, 95
Pagel, B. E. J., Edmunds, M. G., & Smith, G. 1980, MNRAS, 193, 219
Pilyugin, L. S. 2007, MNRAS, 375, 685
Rozas, M. 2007, RevMexAA, submitted
Searle, L. 1971, ApJ, 168, 327
Shields, G. A. 1990, ARA&A, 28, 525
Smith, H. E. 1975, ApJ, 199, 591
Tosaki, T., Shioya, Y., Kuno, N., Nakanishi, K., & Hasegawa, T. 2002, in IAU 8th Asian-Pacific Regional Meeting, Vol. 2, ed. S. Ikeuchi, J. Hearnshaw, & T. Hanawa (Tokyo: Astron. Soc. Jap.), 221
van Zee, L., Salzer, J. J., Haynes, M. P., OḎonoghue, A. A., & Balonek, T. J. 1998, AJ, 116, 2805
Vílchez, J. M., & Pagel, B. E. J. 1988, MNRAS, 231, 257
Zaritsky, D., Kennicutt, R. C., Jr., & Huchra, J. P. 1994, ApJ, 420, 87

M. Rozas: Instituto de Astronomía, Universidad Nacional Autónoma de México, Apdo. Postal 877, 22830 Ensenada, B. C., Mexico (maite@astrosen.unam.mx).